Wind and Structures, Vol. 8, No. 5 (2005) 357-372
DOI: http://dx.doi.org/10.12989/was.2005.8.5.357

Wind effects on a large cantilevered flat roof: loading characteristics and strategy of reduction

J. Y. Fu[†1,2] and Q. S. Li[‡1]

[1]*Department of Building and Construction, City University of Hong Kong, Kowloon, Hong Kong*
[2]*Department of Civil Engineering, Jinan University, Guangzhou 510632, China*

Z. N. Xie[‡†]

Department of Civil Engineering, Shantou University, Shantou 515063, China

(Received January 17, 2005, Accepted May 25, 2005)

Abstract. Mean and extreme pressure distributions on a large cantilevered flat roof model are measured in a boundary layer wind tunnel. The largest peak suction values are observed from pressure taps beneath conical "delta-wing type" corner vortices that occur for oblique winds, then the characteristics and causes of the local peak suctions are discussed in detail. Power spectra of fluctuating wind pressures measured from some typical taps located at the roof edges under different wind directions are presented, and coherence functions of fluctuating pressures are also obtained. Based on these results, it is verified that the peak suctions are highly correlated with the conical vortices. Furthermore, according to the characteristics of wind loads on the roof, an aerodynamic solution to minimize the peak suctions by venting the leading edges and the corners of the roof is recommended. The experimental results show that the suggested strategy can effectively control the generation of the conical vortices and make a reduction of 50% in mean pressures and 25% in extreme local pressures at wind sensitive locations on the roof.

Keywords: flat roof; wind load; wind tunnel test.

1. Introduction

In recent years, more and more long-span structures have been built with increasing span and structural refinement. Roofs of such structures usually have the characteristics of light mass, high flexibility, slight damping and low natural frequency. As the span increases, the natural frequencies generally decrease, and the susceptibility of a roof structure with long-span to resonant excitation by turbulent wind action increases. Consequently, these structures have become progressively more wind sensitive, and therefore it is important to accurately estimate wind loads and wind-induced response of long-span roof structures under strong winds for design purposes.

Investigations on the characteristics of wind loads and wind-induced response of long-span roofs

† Ph. D. Student, E-mail: fjy@jnu.edu.cn
‡ Associate Professor, Corresponding Author, E-mail: bcqsli@cityu.edu.hk
‡† Professor, E-mail: znxie@stu.edu.cn

have been made extensively. For example, Uematsu, *et al*. (1996, 1997, 1999, 2002) estimated the design wind loads for a long-span flat roof and a circular flat roof. Yasui, *et al.* (1999) conducted a response analysis for a long-span structure. In recent years, many large cantilevered roofs have been built around the world. For such structures, there were also a number of wind tunnel investigations conducted. Melbourne (1995) summarized the results of the response of large roof structures through several aeroelastic model studies and proposed an empirical equation for estimating peak design pressure coefficient for cantilevered roofs. However, roof shapes of long-span structures vary widely from structure to structure. It is well known that wind effects on roof structures strongly depend on roof shape and incident wind flow characteristics. Consequently, it is difficult to propose a unified analytical approach to estimate wind loads and wind-induced response of various kinds of long-span roof structures. Therefore, there is a need to carry out comprehensive wind tunnel studies to further the understanding of wind effects on long-span roof structures.

A survey of the damage caused by Typhoon No. 19 in Japan, 1991 revealed that severe damage to roof cladding failure occurred in many low-rise building roofs (Uematsu and Isyumov 1999). It was observed that much of this damage was caused by large local peak suctions on building roofs, in particular on leading edges or corners. So it is important and necessary to clarify the mechanism of occurrence of large peak suctions on roofs and to explore aerodynamic solutions to minimize such wind loads. It has been recognized that the major contribution of wind loading on cantilevered roofs comes from the very large negative pressures generated on the surfaces near the leading edge. Melbourne (1975, 1979) speculated on the cause of the large negative pressures which occur near the leading edge of flat roofs under separated and reattaching flows and, in particular, illustrated the strong dependence of the generation of these pressures on freestream turbulence and how such suction could be reduced by venting the leading edges. One of the relevant applications of a vented leading edge was made for a large cantilevered grandstand roof (Cook 1982). Cook's study (1982) showed that a 25% reduction in mean pressures could be achieved by using a slotted leading edge on a cantilevered grandstand roof. A 1/100 scale aeroelastic model of a cantilevered grandstand roof was tested in a turbulent boundary layer flow over suburban terrain by Melbourne and Cheung (1988) to determine the response of the roof and optimize the leading edge slot configuration in reducing the response. The effectiveness of a leading edge slot was confirmed and it was shown that up to 30% reduction in response could be obtained for a slot width of 5% of the cantilever length which was the optimum configuration.

Previous researches mainly concentrated on seeking the possibility of reducing wind loads on cantilevered grandstand roofs (Cook 1982, Melbourne and Cheung 1988), and in their wind tunnel tests the approaching wind flow was normal to one of the roof edges. However, it has been recognized that the worst fluctuating and negative peak pressures usually occur at edge and roof corner locations for quartering winds. Therefore, there is a need to investigate wind load characteristics on roof structures for oblique wind directions and especially to explore aerodynamic solutions to reduce the large local suctions in such cases. Therefore, in this study, wind tunnel tests are conducted to investigate wind pressure distributions on a large cantilevered flat roof under different wind directions. The objective of this study is to improve understanding of the mechanism contributing to the high suctions near the leading edges and on the corners under conical vortices and consider how to reduce the wind loads. The present paper contains three parts. First, a roof model and wind tunnel experiment arrangements are briefly introduced. Then, the characteristics of wind loads on the roof are presented and discussed on the basis of the wind tunnel measurements. Finally, based on the model test results and Melbourne's suggestion (Melbourne 1979), an attempt is

made to achieve reductions of the peak suctions on the roof by venting the leading edges and corners on the roof, and the effectiveness of the strategy is demonstrated through the obtained wind tunnel test results.

2. Wind tunnel tests

2.1. Experimental arrangements

Wind tunnel experiments were carried out in the boundary layer wind tunnel at Shantou University with a working section 3 m wide×2 m high and 20 m long. Spires and roughness elements were used to generate a simulated atmospheric boundary layer of suburban terrain specified in the China Load Code (GB50009-2001 2002) as exposure B. This terrain type specifies a mean wind speed profile with a power law exponent of $\alpha=0.16$. The measured mean wind speeds and turbulence intensities at various heights over the test section are illustrated in Fig. 1, and it was found that the turbulence intensity was about 18% at the model height. The spectrum of longitudinal wind velocity at the model height is shown in Fig. 2, which agrees with the Davenport type spectrum well.

A flat roof model with square shape shown in Fig. 3 was made to represent a typical large cantilevered roof structure. The roof was erected at a height of 140 mm above the wind tunnel floor. According to the suggestions of Natalini, *et al*. (2002), the thickness of a roof surface where a pressure tap is placed should be at least twice the diameter of the tap, in order to have a well-defined value of the pressure. Considering that there were pressure taps with thickness of 1 mm arranged on the upper and lower roof surfaces, therefore, the roof was made with thickness of 4 mm. The model was made of plexiglass and its dimensions are shown in Fig. 3. Fig. 4 shows a photo of the model mounted in the wind tunnel. The turbulence integral scale was measured to be

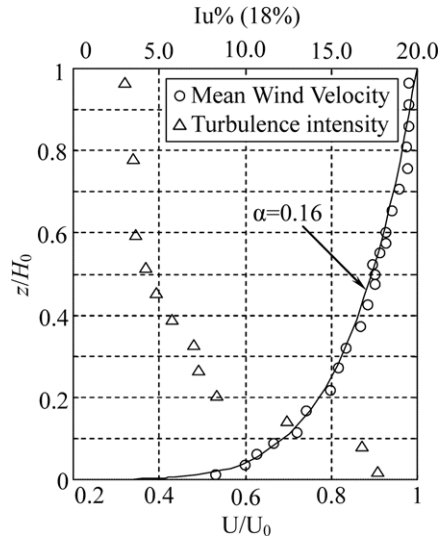

Fig. 1 Mean wind speed and turbulence intensity profiles

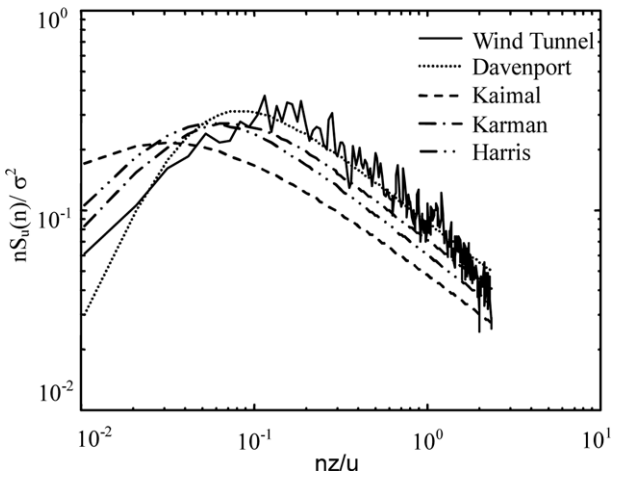

Fig. 2 Spectrum of longitudinal wind velocity at the model height

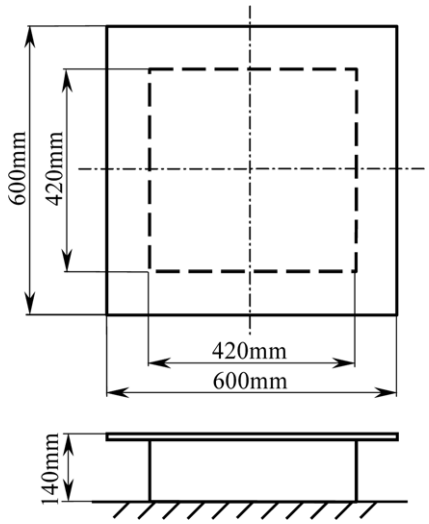

Fig. 3 Model dimensions

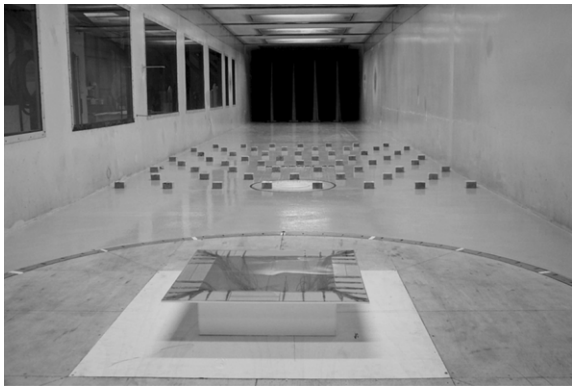

Fig. 4 The model in wind tunnel

45~75 cm at the model height, which should be consistent with the model geometric length scale (Surry 1982, Stathopoulos and Surry 1983, Li and Melbourne 1995, 1999a, 1999b). The geometric length scale of the model was selected as 1:200 so that the turbulence integral scale at the roof height corresponding to the prototype was about 90~150 m, which is consistent with the recommendations of Hunt (1981), AIJ (1996) and Simiu and Scanland (1978). Therefore, the prototype dimensions of the roof are 120 m × 120 m at a height of 28 m.

There were 144 and 108 pressure taps made on the upper and lower roof surfaces, respectively, for pressure measurements. The layout of the pressure taps on the upper roof surface is shown in Fig. 5. In order to obtain the pressure differences between the both sides of the cantilevered roof part, 108 pairs of pressure taps were installed at the same locations on both upper and lower cantilevered roof surfaces, which are marked with ○ shown in Fig. 5. Simultaneous pressure measurements were made from the pressure taps. The other 36 pressure taps marked with ● shown in Fig. 5 were arranged on the upper surface of the enclosed section of the roof.

In the wind tunnel tests, wind direction was defined as an angle β from the east along anti-clockwise direction and β varied from 0^{o} to 360^{o} with increment of 22.5^{o}. Data sampling frequency was 330 Hz with sampling length of 32768, and the measurements were carried out when the mean wind speed at the model height was 10.46 m/s.

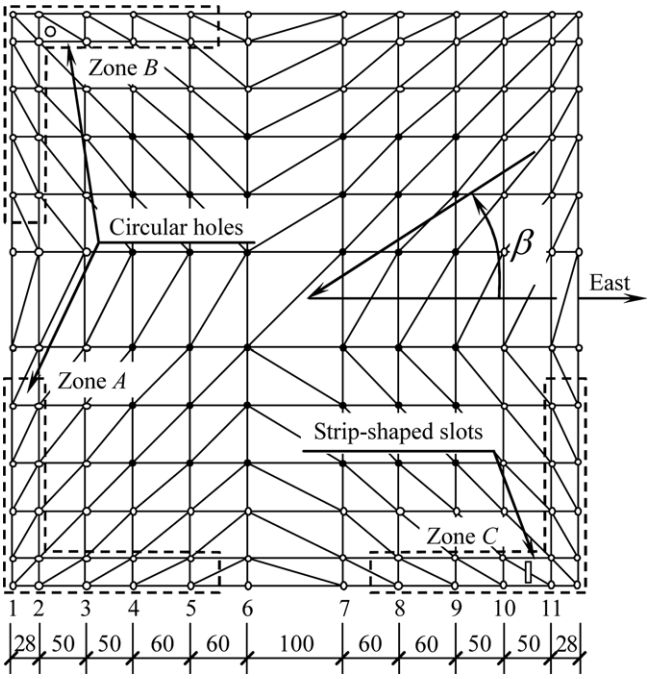

Fig. 5 Layout of the pressure taps on the upper roof surface and aerodynamic solutions to reduction of wind pressures by venting the leading edges and corners of the roof (All dimensions are in millimeters)

2.2. Definitions of parameters

The pressure coefficient of the pressure tap i on the roof surface is defined as follows:

$$C_{pi}(t) = \frac{p_i(t) - p_\infty}{p_0 - p_\infty} \tag{1}$$

where $p_i(t)$ is the measured surface pressure at the tap i; p_0 and p_∞ are the total pressure and the static pressure at reference height, respectively.

The convention for positive roof pressure and the corresponding pressure coefficient, on either the upper or lower roof surface, is always from the air side onto the roof surface. The net wind-induced pressure on the cantilevered roof part due to the combined action of pressures on the upper and lower roof surfaces are defined as positive in the downward direction.

$$\Delta C_{pi}(t) = C^u_{pi}(t) - C^l_{pi}(t) = \frac{p^u_i(t) - p^l_i(t)}{p_0 - p_\infty} \tag{2}$$

where $\Delta C_{pi}(t)$ is the pressure difference coefficient of the tap i between the upper and lower roof surfaces; $p^u_i(t)$ and $p^l_i(t)$ are respectively the measured upper and lower surface pressures at the tap i. In this study, the pressure coefficient $C_{pi}(t)$ defined in Eq. (1) and the pressure difference coefficient $\Delta C_{pi}(t)$ defined in Eq. (2) are both expressed as $C_{pi}(t)$. But, the pressure difference coefficients are used for the cantilevered roof part and the pressure coefficients are used for the upper surface of the enclosed section.

Time-history signals of wind-induced force on a roof surface were obtained from an integration of the simultaneous record of wind pressures over the corresponding surface, and the mean pressure coefficient $\overline{C_p}$ was determined from the pressure measurements. Considering pressure signal attenuation due to the use of tubing systems for pressure measurements, correction to the signal outputs of fluctuating wind pressure is necessary (Xie, *et al*. 2002). The power spectrum of fluctuating wind pressure is determined by

$$S_{Cp}(f) = \frac{S_{Cpx}(f)}{|H(f)|^2} \tag{3}$$

where $S_{Cpx}(f)$ is the signal output of a pressure transducer, and $H(f)$ is the frequency response function of the tubing system.

RMS pressure coefficient C_{prms} and coherence function $\gamma_{xy}^2(f)$ are given by the following equations:

$$C_{prms} = \sqrt{\int_0^\infty S_{Cp}(f)df} = \sqrt{\int_0^\infty \frac{S_{Cpx}(f)}{|H(f)|^2} df} \tag{4}$$

$$\gamma_{xy}^2(f) = \frac{|S_{xy}(f)|^2}{S_x(f)S_y(f)} \tag{5}$$

where $S_x(f)$ and $S_y(f)$ are the power spectra of fluctuating pressures measured from pressure taps x and y, respectively; and $S_{xy}(f)$ is the corresponding cross-power spectrum.

The well-known concept of the peak factor, g, is used in this study to determine the maximum and minimum pressure coefficients ($C_{p\max}$ and $C_{p\min}$) by the following equations.

$$C_{p\max} = \overline{C_p} + gC_{prms} \tag{6}$$

$$C_{p\min} = \overline{C_p} - gC_{prms} \tag{7}$$

If the Normal distribution is adopted for the probability distribution of fluctuating wind pressure, at confidential level of 99.38%, one has $g = 2.5$. However, it has been widely accepted that the probability distribution of fluctuating wind pressure usually does not follow a Gaussian distribution (Li, *et al.* 1999a). In fact, the peak factor depends on position or regions of a structure; it becomes larger than 2.5 in many cases, especially for wind pressure fluctuations at roof corners. The peak factor can be accurately determined from the time history of the measured wind pressures. However, according to the suggestion from Wind Tunnel Testing (1999) among many others, on average it is reasonable to take $g = 3.5$ in engineering applications. Therefore, for the sake of simplicity, $g = 3.5$ is adopted in this study.

The mean local shape factor $\overline{\mu}_{si}$ at the tap i on the roof surface is defined by the following equation:

$$\overline{\mu}_{si} = \overline{C}_{pi}\left(\frac{z_r}{z_i}\right)^{2\alpha} \tag{8}$$

where z_i is the height of the tap i, and z_r is the reference height (1.4 m).

In addition, substituting the maximum or minimum pressure coefficient at the tap i determined from Eq. (6) or (7) into the following equations, we can obtain the corresponding maximum or

minimum local shape factor ($\mu_{s\max i}$ or $\mu_{s\min i}$).

$$\mu_{s\max i} = C_{p\max i}\left(\frac{z_r}{z_i}\right)^{2\alpha} \tag{9}$$

$$\mu_{s\min i} = C_{p\min i}\left(\frac{z_r}{z_i}\right)^{2\alpha} \tag{10}$$

3. Experimental results

3.1. Local shape factor

When wind direction varies from 0° to 360° with incremental step of 22.5°, the roof surfaces were mainly under suction pressures, in particular relatively high negative pressure coefficients occurred at the windward eaves. The critical wind direction was found to be an oblique angle ($\beta = 292.5°$), and Fig. 6 shows the distribution of mean local shape factor on the roof at the critical wind direction. The highest negative pressure with a mean local shape factor of -2.47 was found at the windward corner on the flat roof and the pressure value ($\overline{\mu}_{si}$) decreases from -2.47 to -0.5 from the leading edge to the rear edge on the roof. However, such a high negative pressure region is limited to the regions near the windward roof edges. In other regions, the spatial variation of mean local shape factor is fairly small. Experimental results indicate that the wind pressure coefficients measured under oblique angles are larger than those obtained when wind flow was normal to one of the roof edges.

Explanation for the above observations is associated with flow separation modes along the windward edges of the roof. For an oblique angle, a non-moving type like conical vortices would be formed on a flat roof, as shown in Fig. 7 (Kawai 2002). These vortices glow and decay randomly in

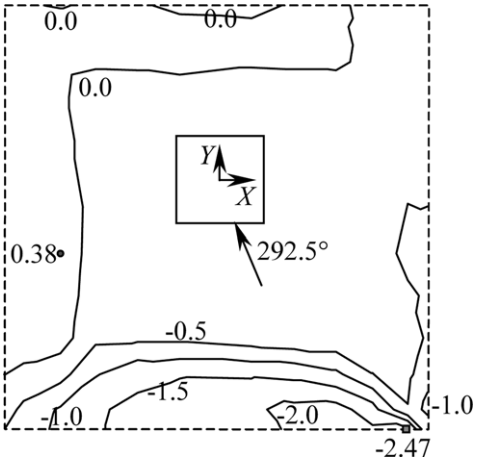

Fig. 6 Contour of the mean local shape factor at the critical wind direction of 292.5°

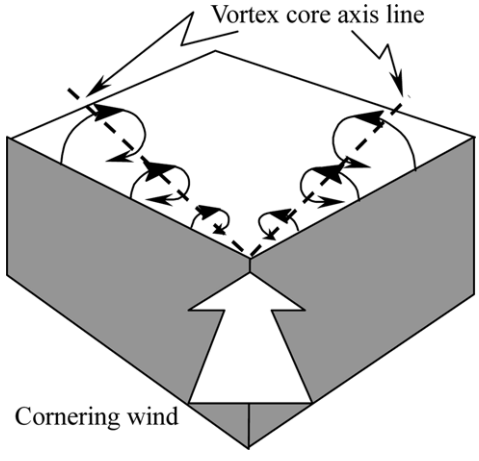

Fig. 7 Conical "delta-wing" corner vortices to induce high negative pressure

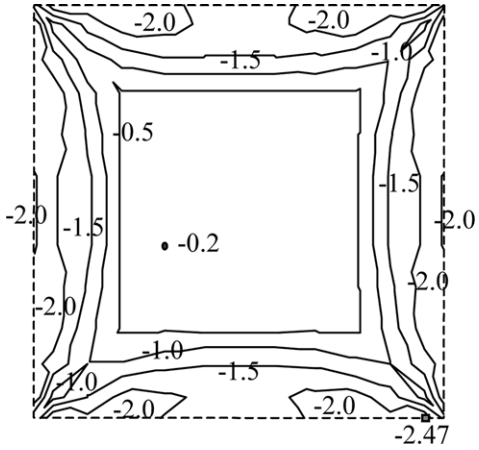

Fig. 8 Contour of the worst negative mean local shape factor for all approaching wind directions

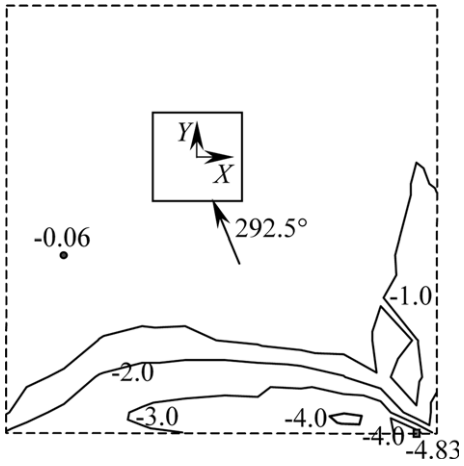

Fig. 9 Contour of the extreme local shape factor at the critical wind direction of 292.5°.

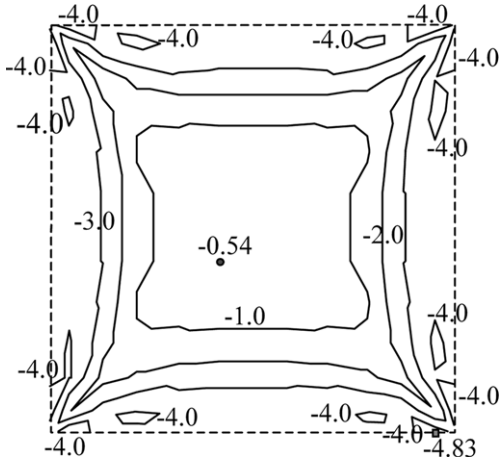

Fig. 10 Contour of the worst negative extreme local shape factor for all approaching wind directions

turbulent wind with change of wind direction and wind speed of the approaching flow, and occasionally become very strong to induce very high negative pressure.

Fig. 8 shows the contour of the worst negative mean local shape factor of each tap for all approaching wind directions. It was found that the four roof corners experienced the worst shape factor of -2.0, and all the shape factor distributions along the eaves were beyond -1.0. But the magnitudes of the local shape factors in the middle parts of the roof were relatively small.

The critical wind direction for the extreme local shape factor distribution is also 292.5°. Fig. 9 and Fig. 10 plot the contour of the extreme local shape factor at the critical wind direction and the contour of the worst negative extreme local shape factor for all the wind directions, respectively. It can be seen from Fig. 9 that the worst negative extreme local shape factor of -4.83 occurred at the windward corner of the roof and its magnitude decreased from -4.83 to -1.0 from the leading edges

to the rear edges on the roof. Results presented in Fig. 10 show that the four roof corners experienced the worst shape factor of -4.0, and the distribution characteristics of the worst negative extreme local shape factor were similar to that of the mean local shape factor shown in Fig. 8.

3.2. Power spectra of fluctuating pressure

Power spectra of fluctuating pressure were determined as a function of the approach wind direction in order to investigate the characteristics of wind-induced pressures on the roof.

Figs. 11(a) and 11(b) show the power spectra of fluctuating pressure difference between the upper and lower roof surfaces for taps 8 and 11 shown in Fig. 5. Tap 8 was located at one of the leading edges of the roof, and the position of tap 11 was at a roof corner. In these figures, in order to observe the actual spectral characteristics varying with frequency and wind direction, the reduced power spectra is expressed as the non-dimensional form, $\{(f \cdot S_{Cp}(f))/(\sigma^2_{\max})\}$, where $\sigma_{\max}$ is the RMS of the maximum C_{prms} experienced over the 16 wind directions, and f denotes frequency.

It can be seen from Figs. 11(a) and 11(b) that the magnitude of pressure spectra which is the indication of the level of energy fluctuation seems to be very small when the two typical taps were under reattaching flows. However, their fluctuating components are relatively large under separated flows.

At higher frequencies, the amplitudes of spectra seem to be very small and the spectral distributions are similar, but there are significant differences in lower frequency range between 1 and 100 Hz in which most of the energy lies and the level of these energy is higher. Measurement results also show that in general the amplitudes of pressure spectra decrease as the frequency increases. However, a small growth in spectral amplitudes at approximately 100 Hz was observed for the two typical taps, which seem to be caused by some electric noise.

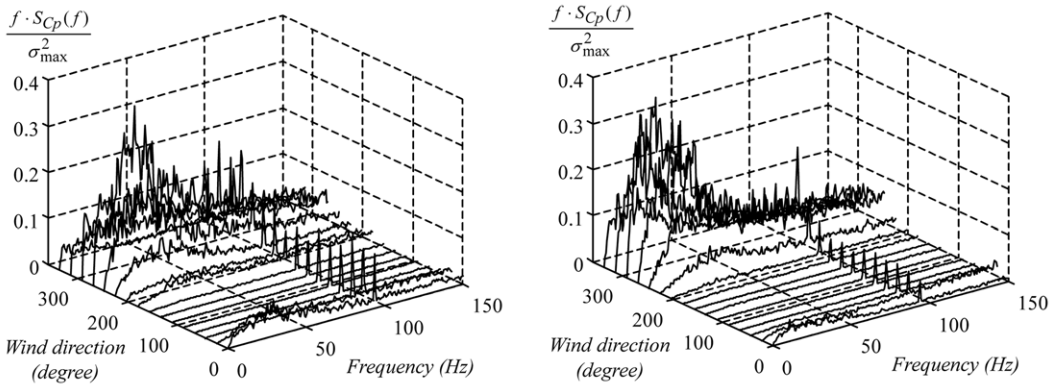

Fig. 11 Power spectra of fluctuating pressure difference between the upper and lower roof surfaces for taps 8 and 11

3.3. Coherence function

For the purpose of obtaining the spatial correlation of fluctuating pressures in frequency domain, coherence functions between fluctuating pressures at various locations were measured.

Figs. 12(a)~(c) show the coherence functions between fluctuating pressures on the surface at the edge of the roof under three wind directions ($\beta = 0^o$) , ($\beta = 270^o$) and ($\beta = 315^o$). The coherence function curves 1, 2, 3, 4, 5, 6, 8, 9 and 10 shown in the three figures were determined from the pressure data from tap 11 and those from taps 1, 2, 3, 4, 5, 6, 8, 9 and 10, respectively. It is seen from Figs. 12(a)~(c) that the values of the coherence functions decrease with increasing frequencies and separating distances.

For $\beta = 0^o$, the values of the coherence function curves shown in Fig. 12(a) associated with frequencies of 20.57, 33.65 and 57.41 Hz were calculated, and the relationship of these values and the distance between the taps was fitted by using an exponential function. Fig. 13 shows the variation of the coherence functions with distances, in which the reference point was set at the location of tap 11 and ξ is the distance from the reference point to the pressure tap concerned.

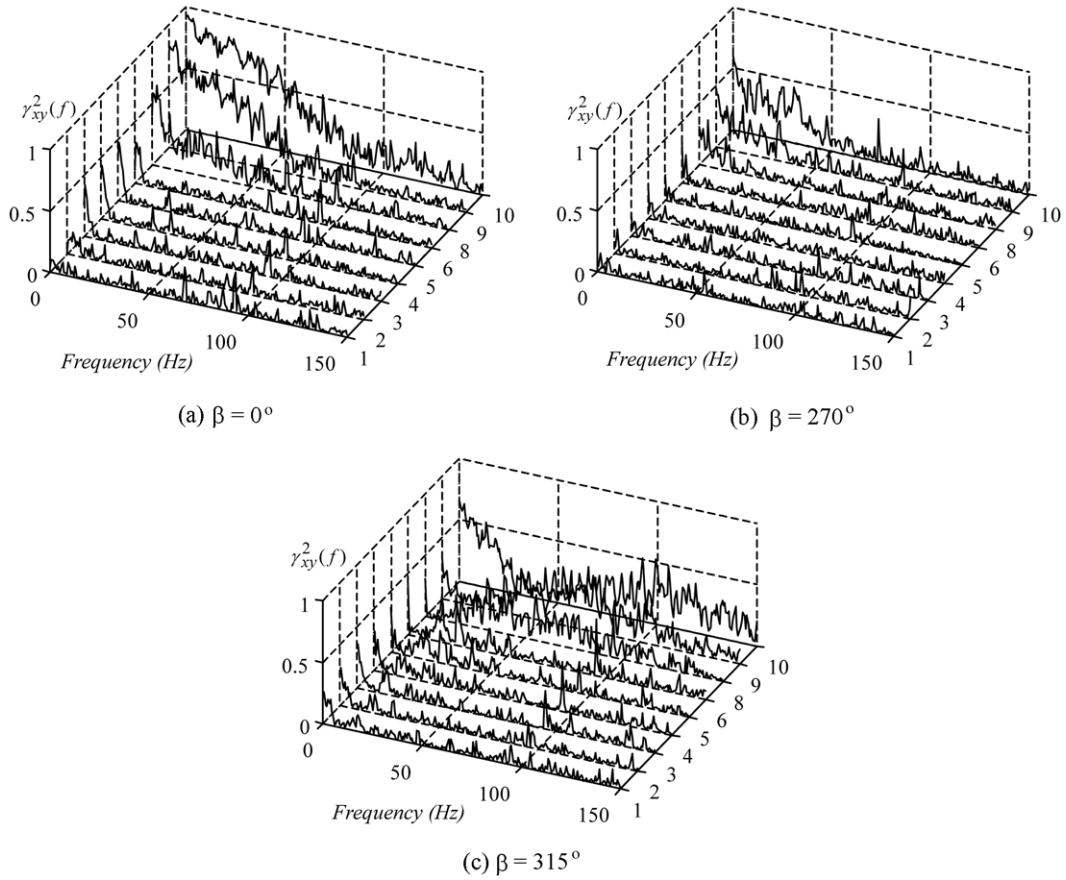

Fig. 12 Coherence functions between fluctuating pressures on the roof surface at the edge of the roof under three wind directions

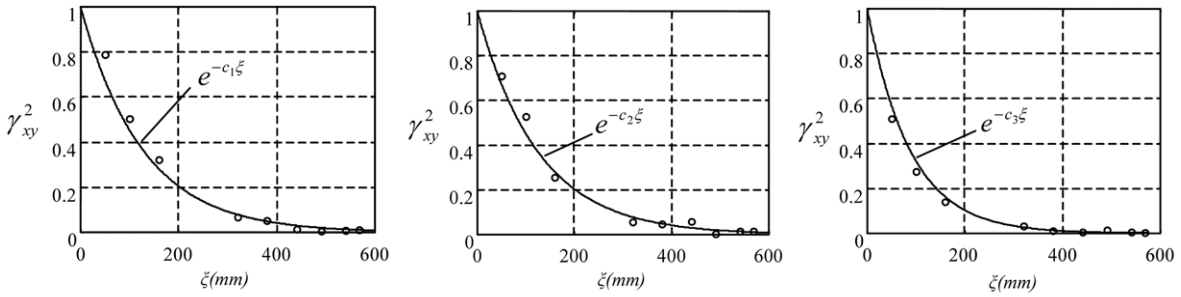

(a) f= 20.57 Hz (b) f= 33.65 Hz (c) f= 57.41 Hz

Fig. 13 Variation of coherence function with distance for $\beta = 0^o$

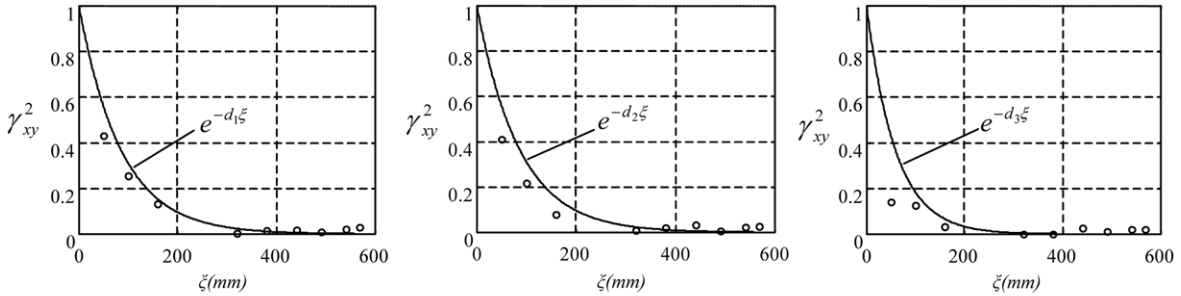

(a) f= 20.57 Hz (b) f= 33.65 Hz (c) f= 57.41 Hz

Fig. 14 Variation of coherence function with distance for $\beta = 270^o$

Figs. 13(a)~(c) show that the values of the coherence functions decay exponentially as the distance between the two taps increases, and the three decay coefficients of the exponential function at frequencies of 20.57, 33.65 and 57.41 Hz are $c_1 = 0.008$ mm^{-1}, $c_2 = 0.008$ mm^{-1}, $c_3 = 0.011$ mm^{-1}, respectively.

For $\beta = 270^o$, the values of the coherence function curves shown in Fig. 12(b) associated with frequencies of 20.57, 33.65 and 57.41 Hz were also calculated, and the relationship of these values and the distance between the taps was also fitted by using the exponential function. Almost the same results were obtained, as shown in Fig. 14.

It can be seen from Figs. 13 and 14 that the variations of the coherence functions with the distance for $\beta = 0^o$ and $\beta = 270^o$ are quite similar, and the three decay coefficients of the exponential function in Figs. 14(a)~(c) are $d_1 = 0.012$ mm^{-1}, $d_2 = 0.012$ mm^{-1}, $d_3 = 0.017$ mm^{-1}, respectively.

The results plotted in Figs. 13 and 14 reveal an important fact, i.e., the decay coefficients along the across-wind direction are larger than those along the along-wind direction. In other words, the correlations of fluctuating pressures along the along-wind direction are higher than those along the across-wind direction, which are consistent with the observation made in Simiu and Scanland (1978).

For $\beta = 315^o$, results were obtained by the similar method, as shown in Fig. 15. However, the relationship of the values of the coherence functions and the distance between the taps was fitted by using a polynomial interpolating function.

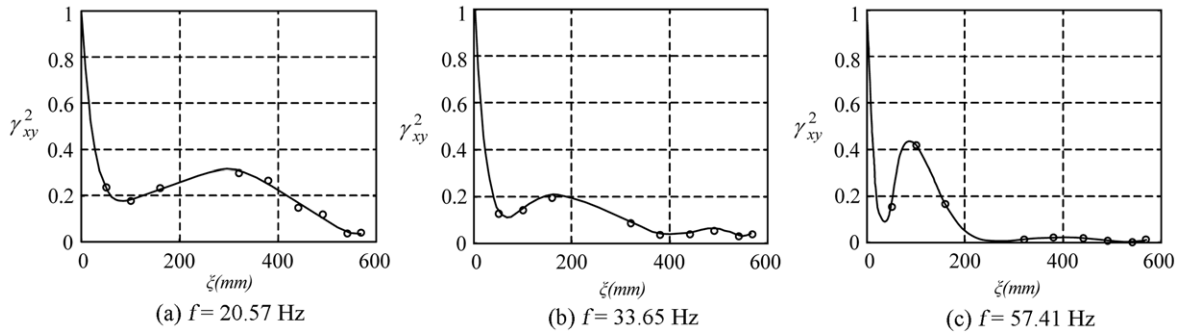

Fig. 15 Variation of coherence function with distance for $\beta = 315^{o}$

It is observed that these values of the coherence functions decrease as the distance increases, but the variation does not follow the exponential function any more, as shown in Figs. 15(a)~(c). The unconventional case should be taken into account in considering the wind loads acting on large cantilevered flat roofs.

Figs. 15(a)~(c) also suggest another important fact, i.e., there are three peaks appeared in these figures; though these peaks are not very obvious. The observed phenomenon may be explained as follows. It is seen from Figs. 15(a)~(c) that the distance between these taps with peaks and the reference point becomes smaller as the frequency increases. In general, large suction fluctuations occurred at windward roof corners in turbulent shear flows are induced by conical vortices, and such fluctuations usually occur in a relatively low frequency range (Kawai and Nishimura 1996), which is consistent with the three selected frequencies in this study. Moreover, correlations of fluctuating pressures between the taps beneath the conical vortices are relatively high (Kawai and Nishimura 1996, Banks, *et al*. 2000). Therefore, it was assumed that the three peaks appeared in Figs. 15(a)~(c) are closely correlated with conical vortices generated on the roof corner, as shown in Fig. 7. It can be seen from Fig. 7 that the frequencies of the conical vortices close to the reference point which is located at the roof corner are higher, i.e., the corresponding sizes of the conical vortices are smaller; on the other hand, the frequencies of the conical vortices far from the reference point are lower, i.e., the corresponding sizes of the conical vortices are larger. Obviously, the results shown in Figs. 15(a)~(c) are consistent with the frequency characteristics of the conical vortices, as shown in Fig. 7. It is thus verified indirectly that the conical vortices would be formed on the roof at an oblique angle.

4. Reduction of wind loads

Aerodynamic stability is one of the most important problems which should be seriously considered in the design of large cantilevered flat roofs. According to the characteristics of wind loads on the roof and based on Melbourne's suggestion (1979), it was decided to make circular holes and strip-shaped slots at the leading edges and the corners of the roof to explore the possibility of reducing wind loads on the large cantilevered flat roof.

Circular holes were made in zone *A* (the diameter of each hole was 1 mm) and zone *B* (the diameter of each hole was 2 mm), as shown in Fig. 5 with holes opening of 2.5% and 5% of the areas of the two zones, respectively. These holes were uniformly distributed over the areas.

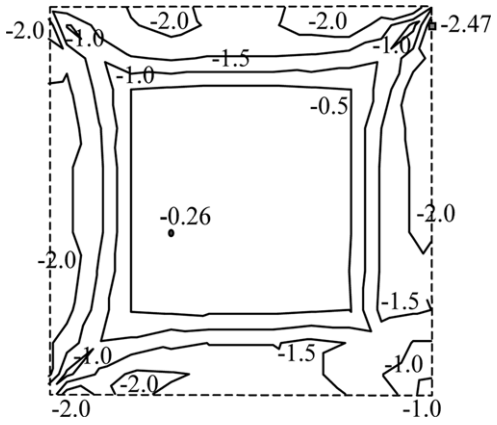

Fig. 16 Contour of the worst negative mean local shape factor for all approaching wind directions with vented arrangements

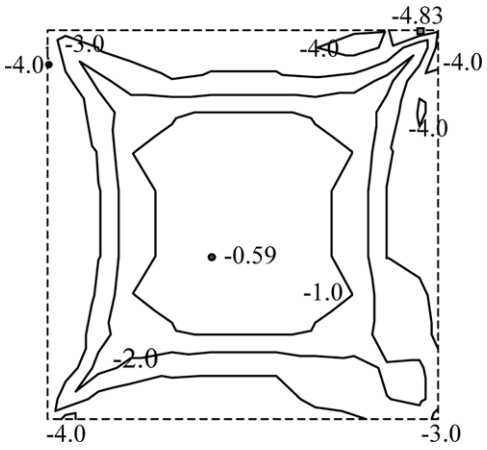

Fig. 17 Contour of the worst negative extreme local shape factor independent of approaching wind direction with vented arrangements

However, the experimental results indicated that the making of the circular holes does not have significant effect on the reduction of wind loads on the roof. This may be due to the fact that the opening ratios of the circular holes are relatively small. However, duo to the model geometric length scale of 1: 200, circular holes with 5% opening ratio were already densely distributed in the relevant areas on the roof. It is thus not meaningful to keep increasing the opening ratio from practical point of view.

The strip-shaped slots were made in zone *C* (the size of each strip-shaped slot was 20 mm×1 mm) with slots opening of 20% of the area, and these slots were also uniformly distributed over zone *C*. Figs. 16 and 17 plot the contours of the worst negative mean local shape factor and the worst negative extreme local shape factor for all approach wind directions, respectively.

It is seen from Figs. 8 and 16 that the values of the contours in the zone *C* decrease from -2.0 to -1.0, indicating that the strip-shaped slots lead to a reduction of the mean local shape factor up to 50%. Comparing Fig. 10 with Fig. 17, it is observed that the values of the contours in the zone *C* reduce from -4.0 to -3.0, implying that the strip-shaped slots result in a reduction of the extreme local shape factor up to 25%. It should be pointed out that Figs. 16 and 17 included the effects of the circular holes. However such effects seem to be not significant.

Similarly, the variation of the coherence function with the distance for $\beta = 315^{o}$ for the case of strip-shaped slots was also measured, as shown in Fig. 18. It was observed that these values of the coherence function can be fitted perfectly by using the exponential function, and the three decay coefficients of the exponential function in Figs. 18(a)~(c) are $e_1 = 0.008\ \text{mm}^{-1}$, $e_2 = 0.008\ \text{mm}^{-1}$, $e_3 = 0.010\ \text{mm}^{-1}$, respectively. This means that the strip-shaped slots can effectively disturb the generation of the conical vortices, and thus reduce the wind loads on the wind sensitive locations of the roof.

Fig. 19 shows the comparison of the power spectra of fluctuating pressure between the case without the slots and the case with the strip-shaped slots under various wind-sensitive directions for taps 10 and 11. It was observed that the energy of the power spectra decreases to a great extent,

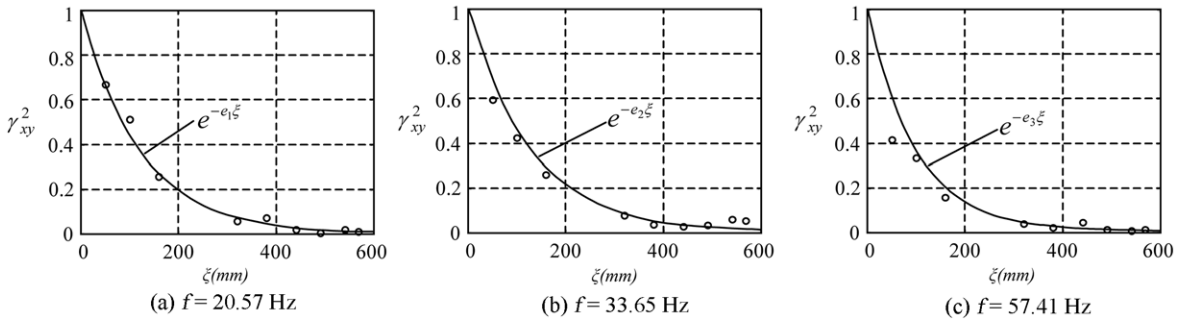

Fig. 18 Variation of coherence function with distance for $\beta = 315^{o}$ for the strip-shaped slots case

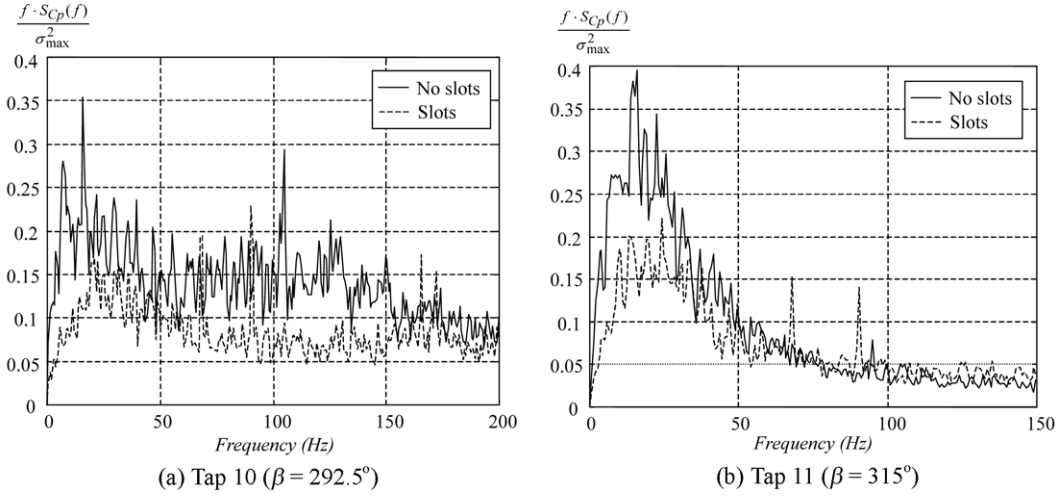

Fig. 19 Comparison of the power spectra of fluctuating pressure

particularly in lower frequency range. All these results indicate that the making of the strip-shaped slots is very effective to reduce wind forces acting the large cantilevered flat roof.

5. Conclusions

The characteristics of wind loads on a large cantilevered flat roof were investigated by wind tunnel experiments. Furthermore, based on Melbourne's suggestion (1979), an attempt was made to reduce the wind loads on the cantilevered flat roof by venting the leading edges and corners of the roof. From the analysis of the experimental results, the following conclusions are summarized.

(1) In general, the design of a large cantilevered roof is dominant by negative wind pressures. Larger mean local shape factors were measured at the windward corner of the roof for oblique approach winds (i.e. $\beta = 292.5^{o}$), and the pressure level decreased rapidly with going downwind to the rear edges of the roof. It was found that these larger negative pressures were highly correlated with the conical vortices formed at the corners of the roof.

(2) The distribution of the extreme local shape factor was very similar to that of the mean local shape factor.
(3) The magnitude of pressure spectra and level of energy fluctuation were very small when the locations of pressure taps were subjected to reattaching flows; however, their fluctuating components were relatively large under separated flows. Most of the fluctuating energy lies in lower frequency range, and the amplitudes of the spectra are usually very small at higher frequencies.
(4) Along the along-wind and across-wind directions, the values of coherence function of fluctuating pressures decay exponentially as the distance between taps increases; and the decay coefficients of the exponential function along the across-wind direction are larger than those along the along-wind direction, i.e., the correlation of fluctuating pressures along the along-wind direction is higher than that along the across-wind direction. For oblique approach winds (i.e. $\beta = 315^{o}$) , the values of the coherence function decrease as the distance increases, but the variation does not follow the exponential function any more, and the frequency domain analysis results indicate that the unconventional case is also highly correlated with the conical vortices.
(5) The circular holes have little effect on the reduction of wind pressures on the roof when the opening ratio is relatively small.
(6) The strip-shaped slots can effectively disturb the generation of the conical vortices and make a reduction of the mean local shape factor and the extreme local shape factor up to 50% and 25%, respectively, at wind sensitive locations of the roof. Meanwhile, the magnitudes of the power spectra of fluctuating wind pressure at some typical taps for wind sensitive directions are also reduced to a great extent.

Acknowledgements

The authors are grateful to the reviewers for their very useful comments and suggestions. The work described in this paper was supported by a grant from Research Grant Council of Hong Kong Special Administrative Region, China (Project No: CityU 1266/03E).

References

AIJ Recommendations for Loads on Buildings (1996), *Architectural Institute of Japan*, Japan. (English version).
Banks, D., Meroney, R.N., Sarkar, P.P., Zhao, Z. and Wu, F. (2000), "Flow visualization of conical vortices on flat roofs with simultaneous surface pressure measurement", *J. Wind Eng. Ind. Aerodyn.*, **84**, 65-85.
Cook, N.J. (1982), "Reduction of wind loads on a grandstand roof", *J. Wind Eng. Ind. Aerodyn.*, **10**, 373-380.
GB50009-2001 (2002), "Load code for the design of building structures", *China Architecture & Building Press*, Beijing. (in Chinese).
Hunt, A. (1981), *Scale Effects on Wind Tunnel Measurements of Wind Effects on Prismatic Buildings,* PhD Thesis, Cranfield Institute of Technology, UK.
Kawai, H. (2002), "Local peak pressure and conical vortex on building", *J. Wind Eng. Ind. Aerodyn.*, **90**, 251-263.
Kawai, H. and Nishimura, G. (1996), "Characteristics of fluctuating suction and conical vortices on a flat roof in oblique flow", *J. Wind Eng. Ind. Aerodyn.*, **60**, 211-225.
Li, Q.S. and Melbourne, W.H. (1995), "An experimental investigation of the effects of free-stream turbulence on streamwise surface pressures in separated and reattaching flows", *J. Wind Eng. Ind. Aerodyn.*, **51-52**, 313-323.
Li, Q.S. and Melbourne, W.H. (1999a), "The effects of large scale turbulence on pressure fluctuations in

separated and reattaching flows", *J. Wind Eng. Ind. Aerodyn.*, **83**, 159-169.
Li, Q.S. and Melbourne, W.H. (1999b), "Turbulence effects on surface pressures of rectangular cylinders", *Wind and Structures,* **2**(4), 253-266.
Li, Q.S., Calderone, I. and Melbourne, W.H. (1999), "Probabilistic characteristics of pressure fluctuations in separated flows for various free-stream turbulence", *J. Wind Eng. Ind. Aerodyn.*, **82**, 125-145.
Melbourne, W.H. (1975), "The relevance of codification to design", *Proc. 4th Int. Conf. on Wind Effects on Building and Structures*, Heathrow, 785-790.
Melbourne, W.H. (1979), "Turbulence effects on maximum surface pressures - a mechanism and possibility of reduction", *Proc. 5th Int. Conf. on Wind Engineering*, Fort Collins, 541-552.
Melbourne, W.H. (1995), "The response of large roofs to wind action", *J. Wind Eng. Ind. Aerodyn.,* **54/55**, 325-335.
Melbourne, W.H. and Cheung, J.C.K. (1988), "Reducing the wind loading on large cantilevered roof", *J. Wind Eng. & Ind. Aerodyn.*, **28**, 410-410.
Natalini, B., Marighetti, J.O. and Natalini, M.B. (2002). "Wind tunnel modeling of mean pressures on planar canopy roof", *J. Wind Eng. & Ind. Aerodyn.*, **90**, 427-439.
Simiu, E. and Scanland, R.H. (1978), *Wind Effects on Structures: An Introduction to Wind Engineering*, New York: John Wiley.
Stathopoulos, T. and Surry, D. (1983), "Scale effects in wind tunnel testing of low buildings", *J. Wind Eng. & Ind. Aerodyn.*, **13**, 313-326.
Surry, D. (1982), "Consequences of distortions in the flow including mismatching scale and intensities of turbulence", *Workshop on Wind Tunnel Modeling for Civil Engineering Applications*. U. S. Dept. of Commerce, National Bureau of Standards, Gaithersburg, MD, U. S. A.
Uematsu, Y. and Isyumov, N. (1999), "Wind pressures acting on low-rise buildings", *J. Wind Eng. Ind. Aerodyn.,* **82**, 1-25.
Uematsu, Y. and Yamada, M. (2002), "Wind-induced dynamic response and its load estimation for structural frames of circular flat roofs with long spans", *Wind and Struct., An Int. J.*, **5**(1), 49-60.
Uematsu, Y., Watanabe, K., Sasaki, A., Yamada, M. and Hongo, T. (1999), "Wind-induced dynamic response and resultant load estimation of a circular flat roof", *J. Wind Eng. Ind. Aerodyn.*, **83**, 251-261.
Uematsu, Y., Yamada, M. and Sasaki, A. (1996), "Wind-induced dynamic response and resultant load estimation for a flat long-span roof", *J. Wind Eng. Ind. Aerodyn.*, **65**, 155-166.
Uematsu, Y., Yamada, M. and Sasaki, A. (1997), "Design wind loads for structural frames of flat long-span roofs: gust loading factor for a structurally integrated type", *J. Wind Eng. Ind. Aerodyn.*, **66**, 155-168.
Wind Tunnel Testing: A General Outline. The Boundary Layer Wind Tunnel Laboratory, The University of Western Ontario, Faculty of Engineering Science, London, Ontario, Canada N6A 5B9, May 1999.
Xie, Z.N., Ni, Z.H. and Shi, B.Q. (2002), "Dynamic characteristics of tubing systems for fluctuating wind pressure measurements", *Chinese Journal of Applied Mechanics*, **19**(1), 5-9. (in Chinese).
Yasui, H., Marukawa, H., Katagiri, J., Katsumura, A., Tamura, Y. and Watanabe, K. (1999), "Study of wind-induced response of long-span structure", *J. Wind Eng. Ind. Aerodyn.,* **83**, 277-288.

CC